Journal of Nuclear Materials 616 (2025) 156023

Contents lists available at ScienceDirect

Journal of Nuclear Materials

journal homepage: www.elsevier.com/locate/jnucmat

Study of the corrosion behaviour of beryllium in solutions representative of Portland cement and magnesium phosphate cement

Sébastien Caes [a,*], Andrey Bukaemskiy [b], Céline Cannes [c], Sylvie Delpech [c], Valdir De Souza [a], Bruno Kursten [a]

[a] Belgian Nuclear Research Centre (SCK CEN), R&D Waste Package, Institute for Sustainable Waste & Decommissioning, Boeretang 200, Mol 2400, Belgium
[b] Forschungszentrum Jülich GmbH, Institute of Fusion Energy and Nuclear Waste Management (IFN-2), Wilhelm-Johnen Straße, Jülich 52428, Germany
[c] Université Paris-Saclay, CNRS/IN2P3, IJCLab, Orsay 91405, France

HIGHLIGHTS

- Worst case scenario study of the Be corrosion in deep geological repository conditions.
- Lower initial beryllium corrosion rate in alkaline pH compare to near neutral pH.
- Few corrosion product on Be surface in OPC solution after one year of corrosion.
- Pitting corrosion observed in solution representative of OPC pore solution.
- Formation of $KBePO_4{\cdot}H_2O$ on Be surface in MPC solution limiting longer-term corrosion.

ARTICLE INFO

Keywords:
Beryllium
Corrosion, EIS
Gas chromatography
SEM
XRD

ABSTRACT

Metallic beryllium is an attractive material for nuclear applications, e.g. thermal reactor and fusion reactors. After use, activated beryllium waste will need to be disposed of in a geological disposal repository. One option for the treatment and conditioning of the beryllium waste could be the direct emplacement of pieces of beryllium in a cementitious matrix. In these conditions, beryllium corrodes due to reaction with water to produce hydrogen, and beryllium hydroxide, leading to possible loss of the waste containment. To gain more information on the anaerobic corrosion of beryllium, Electrochemical Impedance Spectroscopy and hydrogen measurement by gas chromatography were used, while beryllium samples were immersed in solutions representative of promising matrices (Portland cement (OPC, pH 13.5) and magnesium phosphate cement (MPC, pH 8.1)) for maximum one year. At the beginning of the test (< 180 days), both techniques showed that the beryllium corrosion rate was lower in OPC solution than in MPC solution. At longer term (> 180 days), the corrosion rate decreased sharply in MPC solution, while the corrosion rate in OPC solution remained stable. Therefore, at longer term, the lower corrosion rate was observed in MPC solution. The reason of this corrosion rate decrease comes from the formation of a passive layer composed of $Be(OH)_2$ (inner part) and $KBePO_4{\cdot}H_2O$ crystals (outer part) at the surface of beryllium in MPC solution, while no protective corrosion product layer was present on the metal surface in OPC solution. In that later case, pitting corrosion was observed in addition to the dissolution of beryllium species in solution probably in the form of $Be(OH)_4^{2-}$.

1. Introduction

Because of its specific properties, such as a high conductivity of heat and electricity, a high specific strength and stiffness, a low density, a low neutron-capture cross section and a high neutron scattering cross section [1,2], metallic beryllium is an attractive engineering material for nuclear applications, e.g. as moderator, reflector or fuel cladding in thermal reactors [3–6] or breeding blankets and oxygen getter in fusion reactors [7–9]. Inconveniences however are its low fracture toughness [10,11], its high cost [12] and the high toxicity of beryllium and beryllium oxide in particulate form leading to berylliosis and chronic beryllium disease [13–15]. At SCK CEN, the beryllium waste originates

* Corresponding author.
E-mail address: sebastien.caes@sckcen.be (S. Caes).

https://doi.org/10.1016/j.jnucmat.2025.156023
Received 11 February 2025; Received in revised form 24 June 2025; Accepted 2 July 2025
Available online 2 July 2025

from the matrix of the BR2 reactor (cylindrical channels, control rods, reflector plugs). After irradiation, beryllium suffers from embrittlement and swelling, leading to difficulties to recycle the beryllium metal [16,17] and therefore, it is needed to dispose of beryllium as radioactive waste.

Druyts et al. [18] considered that vitrification of beryllium waste in phosphate and glass matrices would be the best option to immobilize radioactive beryllium waste, as these matrices limit the surface area of the waste in contact with water, possess good dissolution resistances and are free of hydrogen production as beryllium will be present in an oxidised form. However, more recent works showed a low corrosion rate of beryllium in neutral to alkaline pH conditions [19–21] as well as a strong uptake of Be(II) species by cementitious matrices [22], leading to a reassessment of cementitious matrices for the final disposal of beryllium wastes, even if a much higher surface area of beryllium waste would be exposed to the immobilisation matrix.

According to the thermodynamic data, beryllium is an amphoteric metal. Recent studies showed that α-$Be(OH)_2$ controls the solubility of beryllium [23]. The domain of stability of the solid α-$Be(OH)_2$ phase, protecting the beryllium surface against active corrosion, depends on the beryllium concentration in solution [19]. At concentration between 10^{-2} to 10^{-6} mol/L, $Be(OH)_2$ is stable at pH between 4.3-7.2 to 11.7-14.5 [19], with the best protection at pH around 12 [20,21]. The use of cementitious matrices with a lower pore solution pH, e.g. calcium sulfoaluminate cement (CSA; pore solution pH around 11.5) or magnesium phosphate cement (MPC; pore solution pH around 8), as well as commonly used ordinary Portland cement (OPC; initial pore solution pH around 13.5) are therefore of interest for the encapsulation of beryllium waste [19,21].

However, the corrosion behaviour of beryllium in conditions representative of deep geological disposal (anaerobic conditions, solutions representative of cementitious pore solution, cement pastes, direct measurement of hydrogen production during corrosion,…), as well as the microstructure of the metal after corrosion have not been deeply studied. Recent work studied the beryllium corrosion in simple solution at different pH [20,24]. However, to our knowledge, no work investigated the analysis of the corrosion rate of beryllium in more complex solution, representative of cementitious materials, appropriated for the disposal of radioactive waste. Such a study could bring important information on the corrosion mechanism of beryllium in cementitious conditioning matrices, as this gives information on the worst case scenario, when no mass transfer limitation nor uptake of Be(II) species by cementitious matrices is present. Therefore, in this work, the corrosion of beryllium was initiated in solutions representative of OPC and MPC in anaerobic argon atmosphere. Different techniques were used to evaluate the corrosion rate, such as electrochemical impedance spectroscopy (EIS) based on the charge transfer resistance and the corrosion current density and, gas chromatography (GC) based on the measurement of the volume of hydrogen produced during corrosion. Other techniques, such as scanning electron microscopy (SEM), X-ray diffraction (XRD) and inductively coupled plasma – mass spectroscopy (ICP-MS) were also used to gain more information on the beryllium samples and on the corroding solutions after the corrosion tests, to allow drawing a possible corrosion mechanism of beryllium in the different studied conditions.

2. Experimental section

2.1. Materials and preparations

S-200-F grade (vacuum hot pressed, <1.5 wt % BeO) beryllium rods (10 cm long and 15 mm in diameter; from BR2, 1980′s campaign, SCK CEN) were used as initial material. Just before use for the corrosion tests, these rods were initially cut under water into ~3 mm thick pellets, using a minitom cutting machine (Struers) and a CBN diamond saw (Bodson Quality Control). After cutting, the pellets were washed with ethanol and milli-Q water. To study the corrosion of beryllium samples by electrochemical techniques, working electrodes were produced by gluing a steel wire on the back side of a beryllium pellet using CW2400 conductive adhesive (Chemtronics). After hardening of the adhesive, a heat-shrunk Teflon® tube was slipped over the steel wire to avoid contact with the test media. Finally, the metallic pellet/steel wire was placed inside a PVC ring and an epoxy resin was poured to insulate completely the connection from the external media. Prior to each electrochemical test, the beryllium electrode was polished to a P1200 SiC emery paper finish using a Minimet 1000 polishing machine (Buehler). Directly after being polished, the electrodes were transferred into a glovebox under argon atmosphere to avoid as much as possible the oxidation of the polished surface.

Note that all manipulation of beryllium (cutting, polishing,…) were done inside a glove bag (Piercan) manufactured especially and exclusively for the work with beryllium, to isolate toxic beryllium particles from the manipulator.

Beryllium corrosion tests were done in solutions representative of ordinary Portland cement pore water (OPC solution) and magnesium phosphate cement pore water (MPC solution). The composition of these solutions is given in Table 1. To mimic the deep geological repository conditions, these solutions were prepared under anaerobic argon atmosphere in a glove box, using degassed milli-Q water.

2.2. Hydrogen measurement by gas chromatography

To measure the hydrogen formed during the corrosion of beryllium, three beryllium pellets were placed in a 1 L leak-tight steel containers coated with a Teflon® liner to avoid the corrosion of steel, filled with 550-700 mL of solution, leading to a S/V ratio close to 22.2 m^{-1} for tests in OPC solution and 27.4 m^{-1} for tests in MPC solution. The detailed information of the beryllium surface area and the volume of solution per container is given in Table SI-1 of the supplementary information. The hydrogen concentration inside the container was measured regularly by a Shimadzu GC-2010 Plus type gas chromatograph (GC) equipment, using a ShinCarbon ST column and a Barrier Discharge Ionisation Detector. The area under the H_2 peak was compared to a calibration curve (from 1 to 10,000 μL/L H_2) to determine the hydrogen concentration. For quality control, a 100 μL/L H_2/Ar gas was injected in the GC before and after each measurement. At the end of the measurement, the atmosphere in the container was purged using three vacuum/argon cycles to remove all hydrogen previously generated. The corrosion reaction of beryllium in water depends on the pH as shown by Eq. (1) to 3 [20].

$$Be + 2\ H_2O \rightarrow Be(OH)_2 + H_2 \quad (For\ 8 < pH < 10.5) \tag{1}$$

$$Be + OH^- + 2\ H_2O \rightarrow Be(OH)_3^- + H_2 \quad (For\ pH > 10.5) \tag{2}$$

$$Be + 2\ OH^- + 2\ H_2O \rightarrow Be(OH)_4^{2-} + H_2 \quad (For\ pH > 10.5) \tag{3}$$

However, for all pH's, when one mole of beryllium is oxidised, one mole of hydrogen is formed. Therefore, by measuring the volume of hydrogen produced over time, collected in 50 mL gas containers, the corrosion rate can be established, assuming a uniform corrosion, using the same calculation in all pH conditions, knowing the volume of the test container headspace, the surface area of beryllium samples (see Table SI-1 in the supplementary information) and the time between two measurements (Table 2).

Table 1
Composition of the solutions used for the corrosion study of beryllium.

Solution composition		Na^+	K^+	SO_4^{2-}	PO_4^{3-}	pH
OPC solution	mol/L	0.14	0.37	2×10^{-3}	–	13.5 ± 0.2
	g/L	3.22	14.47	0.19	–	
MPC solution	mol/L	–	3.76	–	1.98	8.1 ± 0.1
	g/L	–	150.40	–	188.05	

Table 2
Volume of hydrogen produced, corresponding corrosion rate and calculated thickness of corroded beryllium in OPC and MPC solutions.

OPC solution				MPC solution			
Days	Cumulative V H_2 production (L/m^2)	V H_2 between two sampling ($L/m^2 \cdot d$)	Calculated corrosion rate (μm/y)	Days	Cumulative V H_2 production (L/m^2)	V H_2 between two sampling ($L/m^2 \cdot d$)	Calculated corrosion rate (μm/y)
7	0.6	8.4×10^{-2}	6.7	8	1.2	1.6×10^{-1}	12.4
14	1.2	8.6×10^{-2}	6.8	14	2.0	1.1×10^{-1}	8.5
28	2.3	7.9×10^{-2}	6.2	28	3.9	1.3×10^{-1}	10.5
57	4.5	7.5×10^{-2}	6.0	56	7.9	1.4×10^{-1}	11.3
96	6.8	6.0×10^{-2}	4.7	121	18.3	1.6×10^{-1}	12.8
161	9.9	4.8×10^{-2}	3.8	182	28.2	1.6×10^{-1}	12.9
238	11.7	2.3×10^{-2}	1.8	240	30.3	3.6×10^{-2}	2.8
–	–	–	–	308	30.5	3.6×10^{-3}	0.3
364	14.6	2.3×10^{-2}	1.8	365	30.7	2.4×10^{-3}	0.2

2.3. Electrochemical impedance spectroscopy

Electrochemical cell consisted of a working electrode (beryllium; surface area of 0.167 cm^2), a counter electrode (Inconel 625, which was previously passivated in the corresponding electrolyte for a minimum of two weeks), a reference electrode (Ag/AgCl in KCl 0.1 M) and the electrolyte (150 mL of MPC or OPC solution). In these corrosion tests, the S/V ratio was equal to ~1.1. All electrodes were connected to an Autolab PGSTAT 302F potentiostat (Metrohm) combined with the NOVA 2.1.4 version software. EIS spectra were recorded at the open circuit potential (OCP) with a 10 mV amplitude. The evolution of the OCP with time is shown in Figure SI-1 of the supplementary information. The frequency ranged between 10^5 Hz to 10^{-1} Hz, with 10 frequency values per logarithmic decade. To check the system stability, EIS were recorded from high to low frequencies and directly after from low to high frequencies. The analysis and the fit of the spectra were performed using the software 'Zview'. All tests were done in triplicate to evaluate the reproducibility.

2.4. Characterisation techniques

20 mL solution aliquots were sampled at the end of the hydrogen measurement tests to analyse the beryllium concentration by ICP-MS. The measurements were done with a XSERIES2 apparatus (Thermo Scientific, USA) on samples diluted and acidified with 1 % HNO_3. The detection limit for beryllium was <1 μg/L.

SEM-EDS characterisation of the surface of the beryllium samples or the cross section of embedded samples was carried out with a Phenom apparatus (SEM, Phenom PRO X, Thermo Fisher Scientific, The Netherlands) working in a BSE mode and using an accelerating voltage of either 10 kV or 15 kV.

XRD measurements were performed to analyse the surface of the beryllium samples corroded in solution. The measurements were performed using a Bruker©D8 Advance diffractometer operating in Bragg-Brentano configuration and using a Cu-LFF X-ray tube (Cu Kα1 = 0.15405929 nm) at 40 mA and 40 kV. The diffracted X-rays detector was a position-sensitive real time multiple strip detector (Lynxeye) operating in the continuous position-sensitive detection (PSD) mode, with a PSD opening of 3.3°(2θ). The incident beam was collimated by a variable divergence slit set to an illumination length of 15 mm, and axial Soller slits of 2.5°. The diffracted beam passed through the Soller slits and a Ni filter. The beryllium samples were mounted onto a rotating sample stage and diffractograms were recorded while applying a rotation speed of 15 rotations/min. Diffractogram acquisitions were performed by scanning from 5°- 90° with a step size of 0.02° (2θ). The X-ray diffractograms were evaluated with HighScore Plus software 4.9 version software.

3. Results and discussion

3.1. Evolution of the hydrogen production with time during beryllium corrosion

The evolution of the hydrogen production during the corrosion of beryllium in OPC solution (composed of Na^+, K^+ and SO_4^{2-} at pH 13.5) and MPC solution (composed of K^+ and PO_3^{4-} at pH 8.1) was measured during one year (Fig. 1 and Table 2). These tests were used to calculate the corrosion rate of beryllium and to compare them with the results calculated from the electrochemical data.

In OPC solution, the initial production of hydrogen, measured after 7 days of test, reached 84 mL $H_2/m^2 \cdot d$, which corresponds to a corrosion rate close to 7 μm/y, taking the assumption of an uniform corrosion rate. Later on, the hydrogen production rate, and the corresponding corrosion rate, decreased. Finally, the hydrogen production rate reached a steady state at 23 mL $H_2/m^2 \cdot d$ (1.8 μm/y) after 240 days.

In MPC solution, the hydrogen production was initially twice higher (160 mL $H_2/m^2 \cdot d$) than in OPC solution. Later, this production of hydrogen decreased to 110 mL $H_2/m^2 \cdot d$ before to increase again to the initial values until 180 days of test. This hydrogen production corresponds to a corrosion rate around 12 μm/y. However, after 180 days, a sharp decrease of the hydrogen production/corrosion rate was observed until a very low hydrogen production rate, around 2.5 mL $H_2/m^2 \cdot d$ (0.2 μm/y), ten times lower than the one in OPC solution, after 1 year. This decrease of the corrosion rate of beryllium in MPC solution is due to the formation of a protective layer at the surface of the metal. More information about this layer are given in Section 3.2.

At the end of the tests (1 year), 14.6 L H_2/m^2 were produced during the corrosion of beryllium in OPC solution, while 30.7 L H_2/m^2 were produced in MPC solution, showing the general lower corrosion rate in high pH solution. However, looking at the sharp decrease of the hydrogen production at the end of the test in MPC solution, it could be possible that at longer term, the volume hydrogen produced in MPC solution would become lower than in OPC solution. However, longer tests should be performed to assess this hypothesis.

The beryllium concentration in OPC and MPC solutions after the hydrogen measurement tests was analysed by ICP-MS (see Table SI-2 in the supplementary information). Because the surface area of beryllium in contact with the solution is known (assuming a flat surface), it was also possible to calculate the corresponding volume of hydrogen produced from this beryllium concentration in solution. In OPC solution, a production of 12.5 L/m^2 of hydrogen would be produced after one year. This value is relatively similar to the one measured by gas chromatography (14.6 L/m^2, Table 2). This reveals that most of the oxidised beryllium should be released in solution and that the corrosion product layer at the surface of the metallic beryllium should be thin and non-protective. Cannes et al. [20] showed in a solubility diagram that for beryllium concentration ~1 × 10^{-3} mol/L in solution at pH 13.5, the system should be in the passive region in the $Be(OH)_{2\alpha}$ domain. However, these conditions are close to the border between $Be(OH)_2$ domain

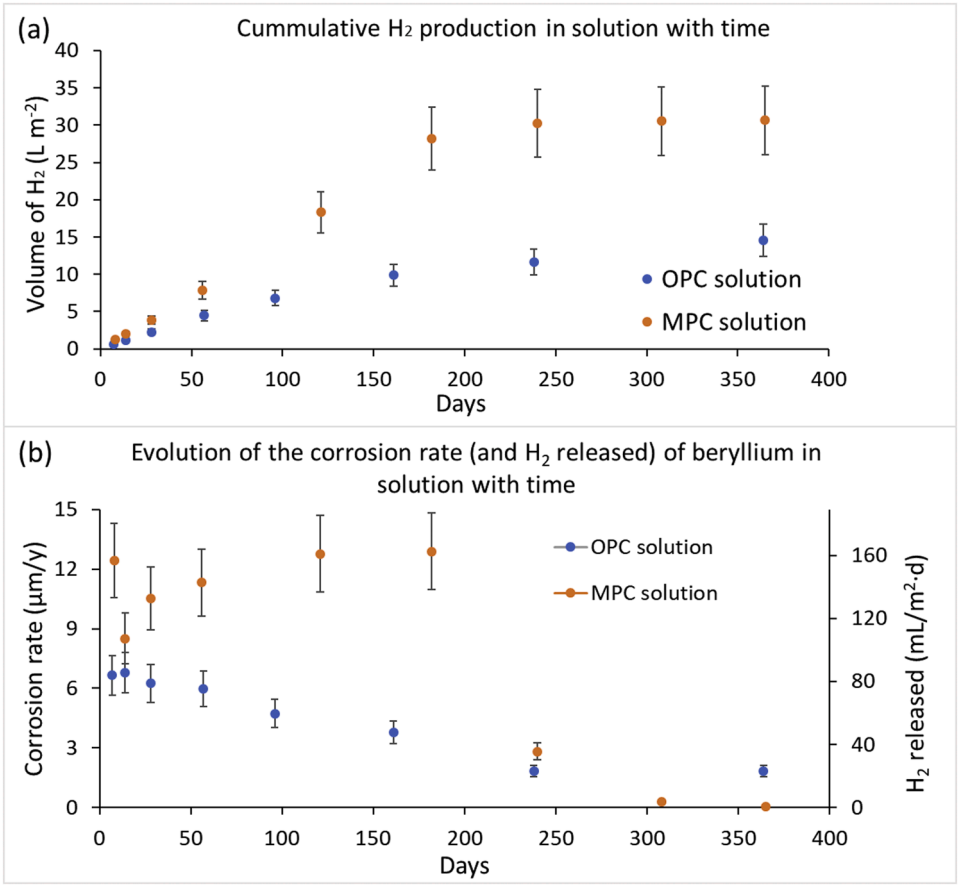

Fig. 1. Leaching tests of beryllium pellets in OPC and MPC solutions. (a) Evolution of the cumulative volume of hydrogen produced with time and (b) Evolution of the corresponding corrosion rate with time. The uncertainty bars represent the propagation of uncertainty.

(passive corrosion region) and $Be(OH)_4^{2-}$ domain (active corrosion region).

The same calculation was done for tests performed in MPC solution: a volume of about 12.2 L/m^2 would be produced after one year. This value is lower than the one measured by gas chromatography (30.7 L/m^2, Table 2). This could be caused by the lower solubility of beryllium in near neutral solution. Indeed, Çevirim-Papaioannou et al. [23,25] showed that the beryllium solubility in NaCl, KCl or $CaCl_2$ at pH 8 could be as low as 10^{-5}–10^{-6} mol/L. Moreover, some crystals were observed at the bottom of the test containers and the surface of the beryllium samples was darker, assuming precipitation of beryllium-based material. Therefore, ICP-MS data underestimated the corrosion rate of beryllium in MPC solution.

3.2. SEM and XRD characterisation

To gain more information on the surface and the cross section of the corroded beryllium pellet, as well as on the precipitates observed at the end of the tests in MPC solution, SEM-EDS and XRD analyses were carried out at the end of the hydrogen measurement tests.

Fig. 2(A-B) shows the surface of the S-200-F grade beryllium pellets, prior to testing. Straight scratches were present on the surface of the samples due to the sawing process used to produce the pellets. Some white particles were also visible, and an EDS analysis (Figure SI-2 of the supplementary information) revealed the presence of Fe, C, Si and Al in these particles, which are impurity elements present in the S-200-F grade beryllium. After one year in OPC solution (Fig. 2(C-D)), even if the scratches initially present were still visible, the whole surface consisted of a crater-like structure due to the presence of pits of 1 to 2 µm in diameter. However, many of these pits coalesced resulting in an increased size until a few tens of micrometres. From the pictures of the cross section (Fig. 2(E-F)), the pits were also visible, revealing a maximum depth of ~25 µm. The presence of these pits is contradictory to the results presented by Sheth et al. [26], mentioning pitting corrosion only in presence of Cl^-, Br^- and I^-. However, such features were also recently observed by Bukaemskiy et al. [24] in NaOH solution at pH above 12.5, without any halides ions. They exposed that these pits initiated at mechanical defects such as impurities, edge of scratches or cavities present at the surface of the sample. No corrosion product layer was observed from the SEM micrographs of the cross section, certainly because it is too thin to be observed by SEM. This confirms that beryllium, when oxidised, was mainly released in solution and does not accumulate at the surface of the metal.

Contrary to the tests in OPC solution, the surface of the beryllium samples corroded for one year in MPC solution was covered by needle-like crystals with a length going from a few hundreds of nanometres up to ~30 µm long (Fig. 2(G-H)). Sometimes, these crystals were found to be organised in a spherical shape. Cross section analyses (Fig. 2(I-J)) confirmed the presence of these crystals organised in a spherical shape, as well as needle-shaped crystals randomly covering the surface of the sample. Cross section analysis also revealed the presence of a corrosion product layer between the beryllium metal and the crystal layer having a thickness ranging from 5 to 20 µm. Even if the detection of beryllium was not possible by EDS, point analyses revealed that the crystals were only composed of K, P and O (and Be; see XRD patterns in Fig. 3), while the corrosion product layer also contained elements such as Mg and Si in small concentration (not shown). Therefore, the corrosion product layer contains elements present as impurities in the beryllium metal, while the crystals consisted of elements only coming from the MPC solution (and beryllium). This could reveal that the crystals precipitates from solution,

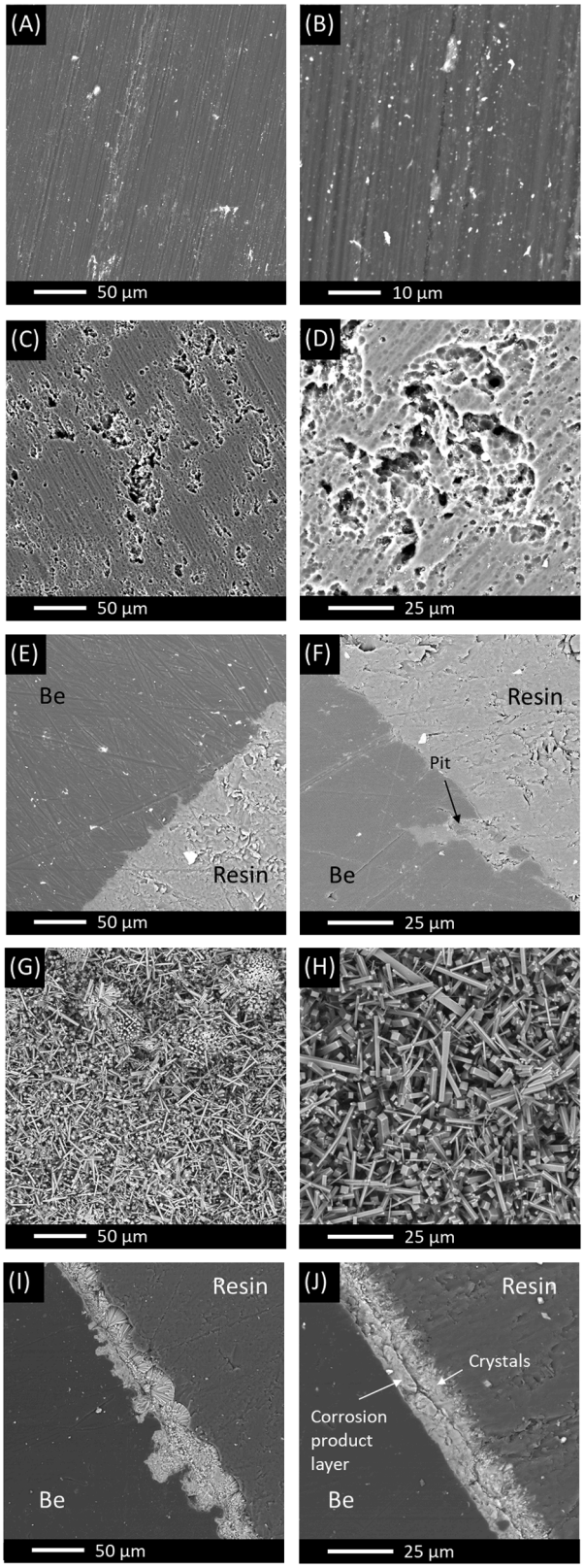

Fig. 2. SEM micrographs of (A-B) the surface of the beryllium samples before corrosion, (C-D) the surface of beryllium samples corroded in OPC solution for one year, (E-F) the cross section of beryllium samples corroded in OPC solution for one year, (G-H) the surface of beryllium samples corroded in MPC solution for one year and (I-J) the cross section of beryllium samples corroded in MPC solution for one year.

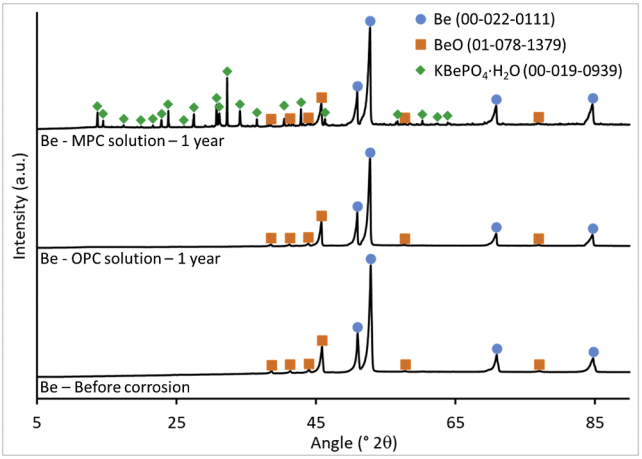

Fig. 3. XRD patterns of beryllium metal before and after one year corrosion in OPC and MPC solutions.

once the concentration of Be(II) species reached the solubility limit, while the corrosion product layer is an accumulation of beryllium hydroxide formed during corrosion of beryllium metal with water.

As mentioned previously, a sharp decrease of the corrosion rate was measured during the hydrogen measurement test after 180 days in MPC solution. The formation of the crystal layer and the corrosion product layer should be the reason of that phenomenon as the access of water to the surface of the beryllium is hindered once these layers covered the entire surface of the metallic samples with a sufficient thickness.

XRD patterns were recorded on beryllium samples before corrosion and after corrosion in OPC and MPC solutions for one year (Fig. 3). Before corrosion, the XRD pattern revealed the presence of metallic beryllium and beryllium oxide. This was expected as the S-200-F beryllium grade is composed of 98.5 % Be and <1.5 wt % BeO. After one year of corrosion in OPC solution, the XRD pattern does not change. This confirms the SEM and ICP-MS results mentioning the very thin $Be(OH)_2$ corrosion product layer formed at the surface of the metallic beryllium. In the MPC solution, in addition to Be and BeO, $KBePO_4{\cdot}H_2O$ (00-019-0939) was also detected. This phase has an orthorhombic crystal structure, corresponding to the needle-like shape of the crystals formed. While the presence of the $Be(OH)_2$ was expected in this sample with regard to the corrosion product layer formed between the metal and the needle-like crystal layer observed by SEM, no peak corresponding to $Be(OH)_2$ was observed. Therefore, if $Be(OH)_2$ is present in the corrosion product layer, it is amorphous. By SEM-EDS, Mg and Si (and Ca) were also found in the corrosion product layer, but no corresponding crystalline phases containing these elements were detected by XRD.

3.3. Electrochemical analysis (EIS) of the corrosion rate

In addition to the evolution of the hydrogen production with time during beryllium corrosion, the corrosion rate was also calculated using EIS. The evolution with time of the Nyquist and Bode diagrams recorded on beryllium electrode immersed in OPC solution (composed of Na^+, K^+ and SO_4^{2-} at pH 13.5) and MPC solution (composed of K^+ and PO_3^{4-} at pH 8.1) is shown in Fig. 4 and Fig. 5, respectively.

The Nyquist diagrams gathered from beryllium immersed in OPC solution are represented by two semi-circles. The one at high frequency corresponds to the impedance of the corrosion product layer present at the surface of the metal and it does not evolve significantly with time (until 135 days of test). This is coherent with previous analyses, showing only a very thin corrosion product layer. At lower frequency, the second semi-circle diameter, corresponding to the impedance of the corrosion process, increased with time. For one occurrence (after 7 days), an induction loop could be observed at high frequency in the Nyquist

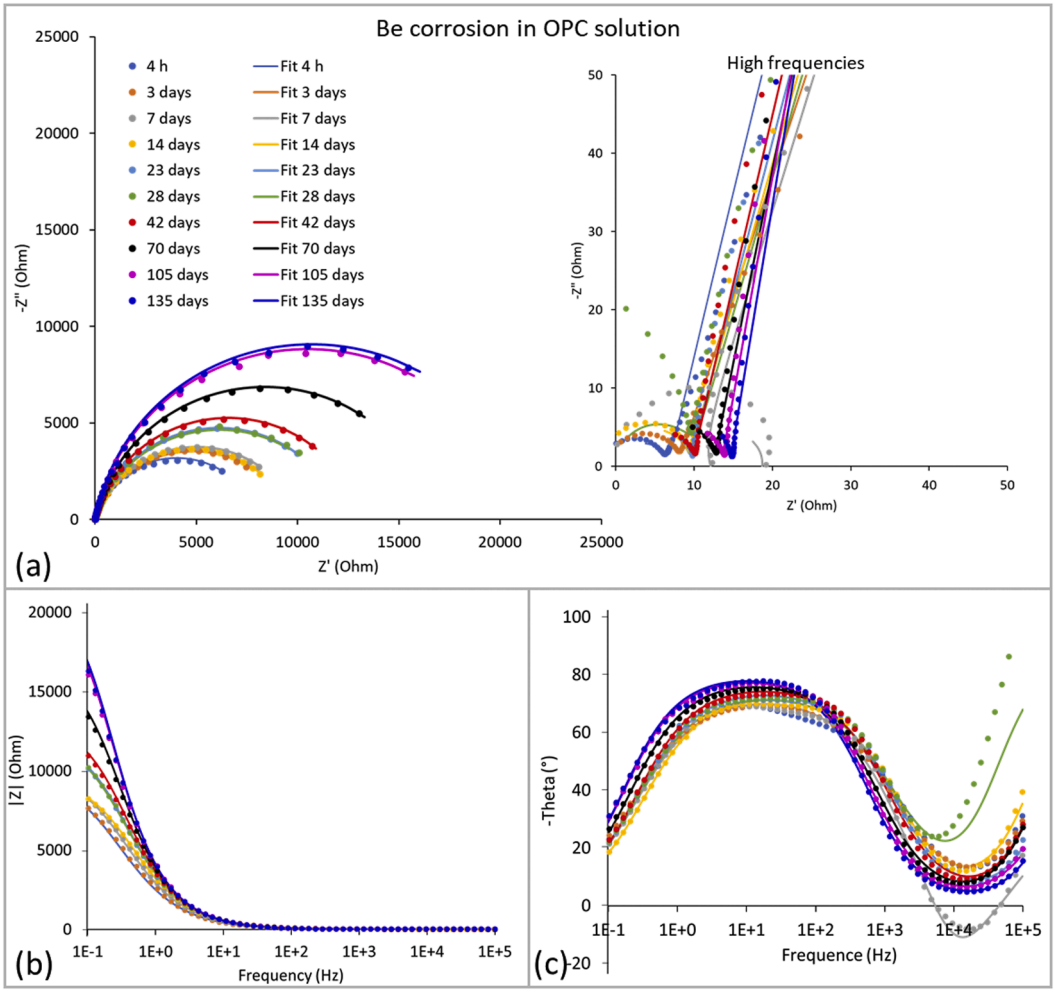

Fig. 4. (a) Evolution of the Nyquist spectra and (b and c) the Bode spectra of beryllium in OPC solution in function of time (dots: experimental results; lines: fit).

diagrams (Fig. 4), but this is supposed to be related to the electrical wires used to connect the studied system to the potentiostat, rather than to the corrosion process. The Bode diagrams also revealed the increase of the impedance modulus with time at low frequencies, while the phase angle remained similar during the entire period of time.

The Nyquist diagrams of beryllium immersed in MPC solution (Fig. 5) are composed of an inductive loop at high frequencies followed by one semi-circle at medium to low frequencies. At low frequencies, contrary to the tests done in OPC solution, the diameter of the semi-circle decreased with time until it stabilise at values close to 8000–9000 Ω. A change in the Bode phase diagram after 77 days in MPC solution was also observed. This could indicate changes at the interface beryllium metal/solution altering the surface of the beryllium metal, such as the initiation of the $KBePO_4{\cdot}H_2O$ crystallisation. However, extra tests are needed to confirm this hypothesis.

To calculate the corrosion rate of beryllium from EIS data, Nyquist and Bode diagrams need to be fitted using an equivalent electrical circuit (EEC), as shown in Fig. 6. This EEC is similar to the one proposed by Cannes et al. [20], and it possesses two R//C circuits in parallel. R_s is used to simulate the resistance of the solution. L_I corresponds to an inductor used to fit the induction loop observed at high frequency in the Nyquist plots. Note that if no induction loop is observed, L_I is omitted from the EEC. The circuit $R_{cpl}//CPE_{cpl}$ is used to model the corrosion product layer observed by SEM at the surface of the beryllium electrode (e.g. the thin product layer at the surface of Be in OPC solution, thick crystal layer at the surface of Be in MPC solution). Finally, CPE_{dl} was added to the EEC to model the double layer capacitance and R_t to model the charge transfer resistance. Note that pure capacitors are replaced by constant phase elements to take into account the heterogeneity of the electrolyte/metal interface observed by SEM in Section 3.2. The fitted values obtained by using this EEC are gathered in Table 3 and are represented by full lines in Fig. 4 and Fig. 5.

Table 3 shows that the impedance mainly comes from the parameters dealing with the corrosion process (CPE_{dl} and R_t), while the resistance of the solutions, and the capacitance and resistance of the corrosion product layer stays low and constant during the whole period of the tests, strengthening the fact that the corrosion product layer is small and non-protective. Note that for tests in MPC solutions, as mentioned earlier, the resistance of the corrosion product layer increases slightly from 77 days onwards (from 5-10 Ω to 165-215 Ω) probably due to the onset of crystallisation of $KBePO_4{\cdot}H_2O$ on the surface of the beryllium samples, at the same time as the increase of the corrosion product layer, once the solubility limit of Be(II) species has been reached in solution. This increase did not modify the charge transfer resistance as crystals and the corrosion product layer were not yet covering entirely the surface of the beryllium electrode with a thick protective layer. Unfortunately, the electrochemical tests were stopped before reaching a possible reduction of the corrosion rate, as observed during the hydrogen measurement test between 180 and 230 days (Section 3.1).

From the fitting data, the corrosion current was calculated using R_t, as described in Delpech et al. [27] and in Eq. (4).

$$I_{corr} = \frac{RT}{n\alpha\mathcal{F}R_t}, \tag{4}$$

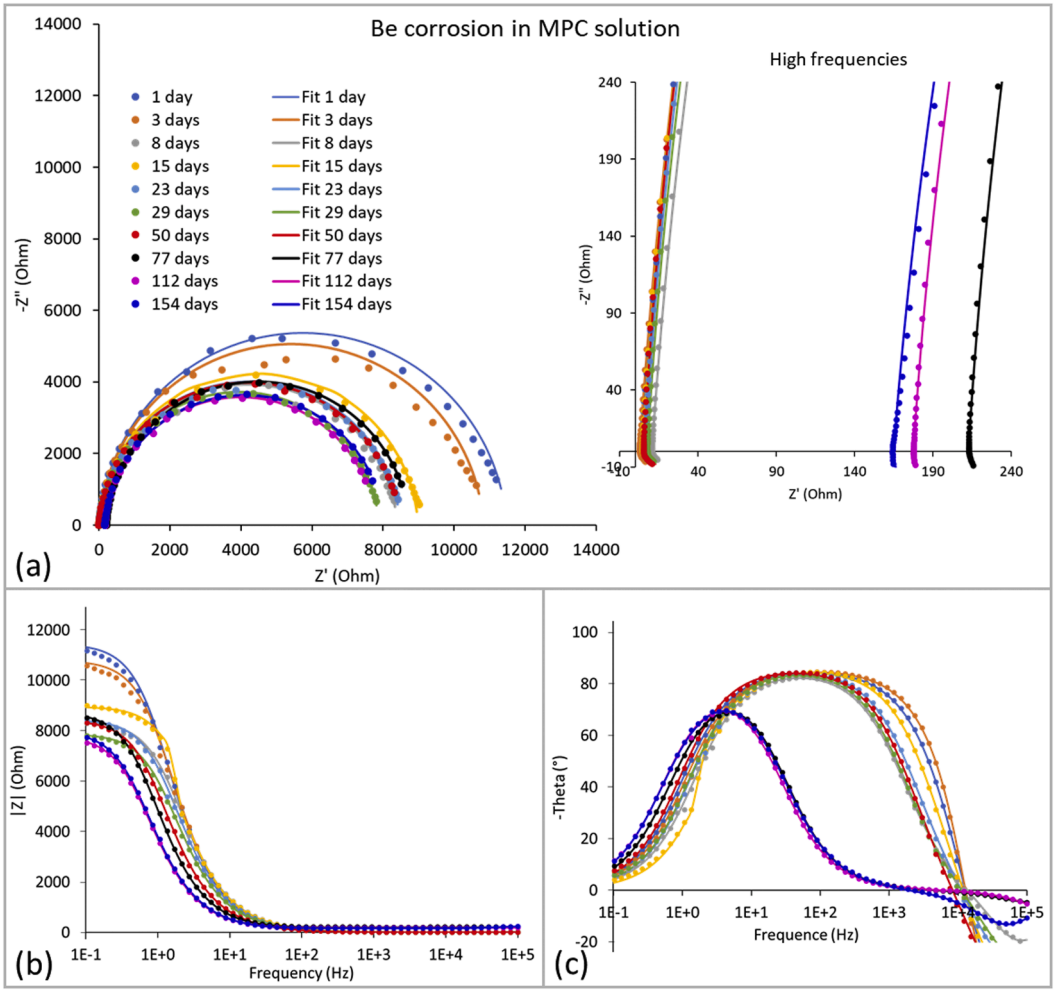

Fig. 5. (a) Evolution of the Nyquist spectra and (b and c) the Bode spectra of beryllium in MPC solution in function of time (dots: experimental results; lines: fit).

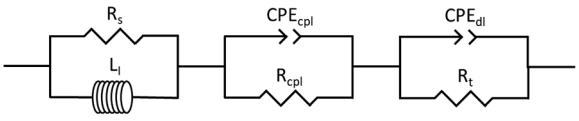

Fig. 6. Equivalent electrical circuits (EEC) used to fit the EIS curves of tests performed (a) in OPC solution and (b) in MPC solution.

where R is the gas constant (J/(K·mol)), T is the temperature (K), n is the number of electrons involved (2 for the oxidation of beryllium), α is the charge transfer coefficient for water reduction (approximated at 0.5 based on the fitting of the $I = f(E)$ stationary curves obtained in water with a Pt electrode), $\mathscr{F}$ is the Faraday constant (C) and R_t is the charge transfer resistance (Ω).

The corrosion current density, i_{corr} (A/cm^2), is given by Eq. (5):

$$\boldsymbol{i_{corr}} = \frac{\boldsymbol{I_{corr}}}{\boldsymbol{S}}, \tag{5}$$

where S is the exposed surface of the electrode (1.767 cm^2 in these tests).

The corrosion rate (v_{corr} in μm/y) is then calculated using Eq. (6):

$$v_{corr} = 3.27 \times 10^6 \times \frac{i_{corr}}{\rho} \times EW, \tag{6}$$

where ρ is the metal density ($\rho_{Be} = 1.85$ g/cm^3) and EW is the equivalent weight. EW is calculated by dividing the atomic weight of an element by the valence of the metal. Hence, for beryllium the atomic weight is 9 and the valence is 2, so EW_{Be} is equal to 4.5.

The evolution of the corrosion rate with time is shown in Fig. 7. Initially, the corrosion rate of beryllium was lower in MPC solution (pH 8.1) than in OPC solution (pH 13.5). However, the corrosion rate in OPC solution decreased with time from 14.5 to 4.9 μm/y., while it increased from 9.6 to ~13-15 μm/y before a steadying at that higher rate after 7 days in MPC solution. Therefore, after 7 days, the corrosion rate became lower in OPC solution than in MPC solution. The corrosion rate values in OPC solution are coherent with the values previously reported at similar pH in NaOH solution [20,24]. Therefore, the addition of sodium, potassium or sulphate in solution or the use of less pure beryllium grade sample do not seem to influence the corrosion rate in alkaline pH. This is also in accordance with Sheth et al. [26], who showed little influence of cations and anions such as NO_3^-, SO_4^{2-}, PO_4^{3-} and F^- on the corrosion rate, at the opposite to Cl^-, Br^- and I^-, which initiate pitting corrosion. The corrosion rates obtained from the corrosion tests done in MPC solution (pH 8.1) are relatively high with regard to the tests performed at that pH in the existing literature [20]. Even if potassium or phosphate ions should have only little influence on the corrosion rate [26], the very high concentration of these ions in the MPC solution could have a detrimental effect on the corrosion of beryllium. Another hypothesis could be that the lower purity of the S-200-F grade samples used in this research could react more in these near neutral pH solutions. At the end of the test (4-5 months), the corrosion of beryllium was three times lower in OPC solution (high pH) than in MPC solution (near neutral pH). Cannes et al. [20] also analysed the corrosion of beryllium in different

Table 3
Fitting data of the EIS spectra of beryllium.

Tests in OPC solution	Days	R_s (Ω)	L (Henry)	CPE_{cpl}		R_{cpl} (Ω)	CPE_{dl}		R_t (Ω)
				K_1 ($F{\cdot}S^{\alpha}$)	α_{cpl}		K_{dl} ($F{\cdot}S^{\alpha}$)	α_{dl}	
	0.2	6.6×10^{-8}	/	8.8×10^{-7}	0.89	6.7	9.7×10^{-5}	0.86	8010
	3	1.7×10^{-7}	/	3.7×10^{-7}	0.91	8.1	8.1×10^{-5}	0.80	9690
	7	1.6×10^{-10}	1.1×10^{-4}	9.6×10^{-8}	1	10.1	6.7×10^{-5}	0.82	10,040
	14	2.4×10^{-8}	/	1.8×10^{-7}	0.97	9.2	5.6×10^{-5}	0.83	9640
	23	4.8×10^{-7}	/	5.9×10^{-8}	1	9.3	5.3×10^{-5}	0.84	12,210
	28	1.0×10^{-7}	/	4.0×10^{-7}	1	9.5	5.5×10^{-5}	0.83	12,300
	42	1.9×10^{-6}	/	8.3×10^{-8}	1	9.7	5.0×10^{-5}	0.86	13,130
	70	2.1×10^{-2}	/	6.4×10^{-8}	1	12.3	4.7×10^{-5}	0.88	16,720
	105	2.8×10^{-7}	/	1.5×10^{-7}	1	13.6	4.5×10^{-5}	0.89	20,980
	135	1.4×10^{-8}	/	2.8×10^{-8}	1	14.5	4.5×10^{-5}	0.90	21,340
Tests in MPC solution	Days	R_s (Ω)	L (Henry)	CPE_{cpl}		R_{cpl} (Ω)	CPE_{dl}		R_t (Ω)
				K_{cpl} ($F{\cdot}S^{\alpha}$)	α_{cpl}		K_{dl} ($F{\cdot}S^{\alpha}$)	α_{dl}	
	1	13.8	1.7×10^{-5}	1.0×10^{-7}	0.9	3.0	1.5×10^{-5}	0.96	11,480
	3	14.6	1.8×10^{-5}	1.0×10^{-7}	0.9	2.4	1.4×10^{-5}	0.96	10,830
	7	11.2	1.6×10^{-5}	1.0×10^{-8}	0.9	10.5	1.4×10^{-5}	0.96	8390
	15	11.5	2.0×10^{-5}	1.0×10^{-8}	0.9	4.4	1.4×10^{-5}	0.96	8980
	23	11.0	2.0×10^{-5}	1.0×10^{-8}	0.9	6.3	1.6×10^{-5}	0.96	8470
	29	12.9	1.8×10^{-5}	1.0×10^{-8}	0.9	7.6	1.7×10^{-5}	0.96	7870
	50	16.1	2.4×10^{-5}	1.0×10^{-8}	0.9	5.0	2.2×10^{-5}	0.97	8430
	77	36.4	4.7×10^{-5}	1.0×10^{-10}	0.9	212.4	2.9×10^{-5}	0.96	8530
	112	61.8	2.9×10^{-5}	1.0×10^{-10}	0.9	177.3	4.1×10^{-5}	0.96	7620
	154	96.7	2.4×10^{-4}	5.0×10^{-10}	0.9	164.9	4.0×10^{-5}	0.95	7870

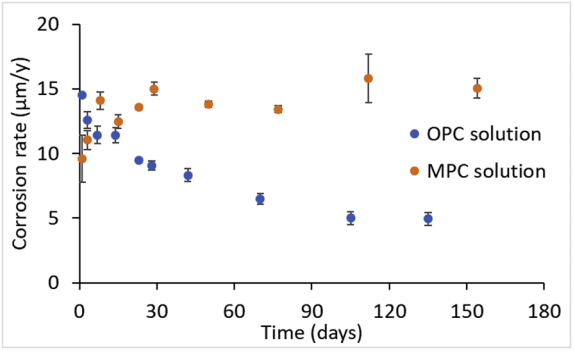

Fig. 7. Evolution of the corrosion rate of beryllium with time in OPC and MPC solutions. The uncertainty bars represent the propagation of uncertainty.

pH solutions composed of HCl and NaOH and the charge transfer resistance at pH ~8 was also lower (and therefore the corrosion rate higher) than the one expected at pH 13.5 (only measured at pH 13 and 14 in [20]). Note that, a good correlation between both techniques was observed, proving the consistency of the tests, even if the corrosion rates calculated from the fit of the EIS data are slightly higher than the ones calculated from the production of hydrogen. In addition to the fact that higher corrosion rate calculated from electrochemical techniques is commonly reported, the lower S/V ratio in these tests (~1.2 m^{-1} vs. ~25 m^{-1}) could also explain this difference.

4. Conclusions

Because of its physico-chemical properties, metallic beryllium is an attractive engineering material for nuclear applications. However, after irradiation, these properties are altered (embrittlement, swelling,…) and the disposal of beryllium as radioactive waste is needed. In this context, the corrosion of non-irradiated metallic beryllium, in conditions representative of geological disposal of nuclear waste is of interest. As a preliminary study, corrosion tests in solution can help bringing important information on the corrosion mechanism of beryllium in cementitious conditioning matrices, as this gives information on the worst case scenario, when no mass transfer limitation nor uptake of Be (II) species by cementitious matrices is present. In the literature, test in simple solution, such as HCl or NaOH were reported. However, to our knowledge, the corrosion rate of beryllium in solution representative of cementitious matrix was never published. Therefore, the corrosion of S-200-F beryllium grade, used as moderator in the BR2, was evaluated in solutions representative of ordinary Portland cement paste (OPC solution) and magnesium phosphate cement paste (MPC solution), as those cement pastes/mortars are possible options to dispose of these wastes. Different techniques, such as EIS, hydrogen measurement by gas chromatography and measurement of beryllium concentration in solution by ICP-MS were used to determine the corrosion rate of beryllium. Moreover, at the end of the tests, SEM and XRD were used to characterise beryllium samples after corrosion.

The main conclusions of this work are given here below:

1. Two independent measurement methods, showed similar corrosion rates, in both trends and numerical values, for tests performed in similar conditions (beryllium in OPC solution or in MPC solution). Moreover, these corrosion rates were relatively low, revealing the possibility of using OPC and/or MPC cement pastes for the disposal of metallic beryllium waste. Corrosion of beryllium directly immersed in cementitious materials will be the subject of a next publication.
2. Initially, the corrosion rate was higher if beryllium was immersed in MPC solution (K^+, PO_4^{3-}, pH 8.1) compared to the OPC solution (Na^+, K^+, SO_4^{2-}, pH 13.5). After 4–5 months, the corrosion rate was three time lower in OPC solution (~5 µm/y compared to ~15 µm/y in MPC solution). However, after 180 days (~6 months) in the hydrogen measurement tests, the corrosion rate of beryllium in MPC solution dropped sharply, due to the thickening of a corrosion product layer and to the crystallisation of $KBePO_4{\cdot}H_2O$ on the metal surface, once the solubility limit of Be(II) species in solution reached the solubility limit, passivating the surface of beryllium. The formation of these layer and crystals could also be responsible of changes recorded in the EIS Bode spectra after 50 days of tests.
3. After corrosion in OPC solution, pitting corrosion of beryllium was observed with pit size of 1 to 2 µm in diameter. However, many of these pits coalesced resulting in an increased size until a few tens of micrometres. The SEM analysis of the cross section of the sample revealed pit depth reaching up to ~25 µm.
4. In OPC solution, very little $Be(OH)_2$ was present at the surface of the metal, meaning that the corrosion product was dissolved in solution

probably in the form of $Be(OH)_4^{2-}$. In MPC solution (at pH 8.1), the solubility of Be(II) species is lower. After reaching saturation, a corrosion product layer and $KBePO_4{\cdot}H_2O$ crystals grew at the surface of beryllium. EDS analysis revealed the presence of impurity elements from the S-200-F beryllium sample, such as Mg and Si in the corrosion product layer but not in the crystals.

CRediT authorship contribution statement

Sébastien Caes: Writing – original draft, Visualization, Validation, Investigation, Data curation, Conceptualization. **Andrey Bukaemskiy:** Writing – review & editing, Validation. **Céline Cannes:** Writing – review & editing, Validation. **Sylvie Delpech:** Writing – review & editing, Validation. **Valdir De Souza:** Writing – review & editing. **Bruno Kursten:** Writing – review & editing.

Declaration of competing interest

The authors declare that they have no known competing financial interests or personal relationships that could have appeared to influence the work reported in this paper.

Acknowledgements

The authors would like to acknowledge Ben Gielen, Sabrina Lunardi, Pieter Schroeders, Steven Smets and Wim Verwimp for the technical support. This project has received funding from the Euratom research and training programme 2020–2024 under grant agreement No 945098 (PREDIS) and was also done in the broader framework of a public-public partnership between SCK CEN and ONDRAF/NIRAS.

Supplementary materials

Supplementary material associated with this article can be found, in the online version, at doi:10.1016/j.jnucmat.2025.156023.

Data availability

Data will be made available on request.

References

[1] L. Alderighi, P. Gans, S. Midollini, A. Vacca, Aqueous solution chemistry of beryllium, in: A.G. Sykes, A. Cowley (Eds.), Main Chemistry Group, Advances in Inorganic Chemistry, Main Chemistry Group, Advances in Inorganic Chemistry, 50, Academic Press, San Diego, 2000, pp. 110–172.
[2] K.A. Walsh, Beryllium Chemistry and Processing, ASM International, 2009, https://doi.org/10.31399/asm.tb.bcp.9781627082983.
[3] D. Chandler, R.T. Primm, G.I. Maldonado, Reactivity accountability attributed to beryllium reflector poisons in the high flux isotope reactor, in: ORNL Report TM-2009/188, Oak Ridge, USA, 2009.
[4] D. Chandler, G.I. Maldonado, L.D. Proctor, R.T. Primm, Nuclear transmutations in HFIR's beryllium reflector and their impact on reactor operation and reflector disposal, Nucl. Tech. 177 (2012) 395–412, https://doi.org/10.13182/NT12-A13483.
[5] J.M. Beeston, Beryllium metal as a neutron moderator and reflector material, Nucl. Eng. Des. 14 (1970) 445–474, https://doi.org/10.1016/0029-5493(70)90161-5.
[6] L.L. Snead, S.J. Zinkle, Use of beryllium and beryllium oxide in space reactors, AIP Conf. Proceed. 746 (2005) 768, https://doi.org/10.1063/1.1867196.
[7] H. Kawamura, S. Tanaka, E. Ishitsuka, in: Proceedings of the Sixth IEA International Workshop on Beryllium Technology for Fusion, Miyazaki, Japan, 2004.
[8] J.H. Kim, S. Nakano, M. Nakamichi, A novel method to stably secure beryllium resources for fusion blankets, J. Nucl. Mater. 542 (2020) 152522, https://doi.org/10.1016/j.jnucmat.2020.152522.
[9] J.S. Park, X. Bonnin, R. Pitts, Assessment of ITER divertor performance during early operation phases, Nucl. Fusion 61 (2021) 016021–016035, https://doi.org/10.1088/1741-4326/abc1ce.
[10] H. Conrad, J. Hurd, D. Woodard, The fracture toughness of beryllium, J. Test. Eval. 1 (1973) 88–89, https://doi.org/10.1520/JTE10883J.
[11] W.O. Shabbits, W.A. Logsdon, S-200 grade beryllium fracture toughness properties, J. Test. Eval. 1 (1973) 110–118, https://doi.org/10.1520/JTE10885J.
[12] J.S. Punni, M.J. Cox, The effect of impurity inclusions on the pitting corrosion behaviour of beryllium, Corros. Sci. 52 (2010) 2535–2546, https://doi.org/10.1016/j.corsci.2010.03.024.
[13] S. Bolan, H. Wijesekara, M. Tanveer, V. Boschi, L.P. Padhye, M. Wijesooriya, L. Wang, T. Jasemizad, C. Wang, T. Zhang, J. Rinklebe, H. Wang, S.S. Lam, K.H. M. Siddique, M.B. Kirkham, N. Bolan, Beryllium contamination and its risk management in terrestrial and aquatic environmental settings, Environ. Pollut. 320 (2023) 121077, https://doi.org/10.1016/j.envpol.2023.121077.
[14] J. Elguero, I. Alkorta1, The dubious origin of beryllium toxicity, Struct. Chem. 34 (2023) 391–398, https://doi.org/10.1007/s11224-023-02130-2.
[15] H. TenHarmsel, L. Wang, C. Dumas, K.D. Rosenman, Mortality among individuals diagnosed with chronic beryllium disease and beryllium sensitization, J. Occup. Environ. Med. 66 (2024) 247–251, https://doi.org/10.1097/JOM.0000000000003033.
[16] F. Moons, R. Chaouadi, J.L. Puzzolante, Fracture behaviour of neutron irradiated beryllium, Fusion Eng. Des. 41 (1998) 187–193, https://doi.org/10.1016/S0920-3796(98)00137-9.
[17] V. Chakin, R. Rolli, H.C. Schneider, P. Kurinskiy, W.V. Renterghem, Pores and cracks in highly neutron irradiated beryllium, J. Nucl. Mater. 416 (2011) 3–8, https://doi.org/10.1016/j.jnucmat.2010.11.098.
[18] F. Druyts, P. Van Iseghem, Conditioning methods for beryllium waste from fusion reactors, Fusion Eng. Des. 69 (2003) 607–610, https://doi.org/10.1016/S0920-3796(03)00169-8.
[19] P. Bouhier, C. Cannes, D. Lambertin, C. Grisolia, D. Rodrigues, S. Delpech, Evaluation of several conditioning matrices for the management of radioactive metal beryllium wastes, J. Nucl. Mater. 559 (2022) 153464, https://doi.org/10.1016/j.jnucmat.2021.153464.
[20] C. Cannes, P. Bouhier, D. Lambertin, C. Grisolia, D. Rodrigues, S. Delpech, Reactivity of beryllium in aqueous solution from acidic to basic pH, J. Electroanal. Chem. 950 (2023) 117879, https://doi.org/10.1016/j.jelechem.2023.117879.
[21] R. Laflotte, C. Cau-Dit-Coumes, J. Haas, D. Rodrigues, C. Cannes, S. Delpech, M. Rivenet, Stabilization and solidification of beryllium waste: influence of the cement composition on the corrosion of Be metal, Materials 17 (2024) 5401, https://doi.org/10.3390/ma17225401.
[22] B. Grambow, M. Lòpez-García, J. Olmeda, M. Grivé, N.C.M. Marty, S. Grangeon, F. Claret, S. Lange, G. Deissmann, M. Klinkenberg, D. Bosbach, C. Bucur, I. Florea, R. Dobrin, M. Isaacs, D. Read, J. Kittnerová, B. Drtinová, D. Vopálka, N. Çevirim-Papaioannou, N. Ait-Mouheb, X. Gaona, M. Altmaier, L. Nedyalkova, B. Lothenback, J. Tits, C. Landesman, S. Rasamimanana, S. Ribet, Retention and diffusion of radioactive and toxic species on cementitious systems: main outcome of the CEBAMA project, Appl. Geochem. 112 (2020) 104480, https://doi.org/10.1016/j.apgeochem.2020.104480.
[23] N. Çevirim-Papaioannou, X. Gaona, M. Böttle, E.Yalçintaş Bethune, D. Schild, C. Adam, T. Sittel, M. Altmaier, Thermodynamic description of Be(II)solubility and hydrolysis in acidic to hyperalkaline NaCl and KCl solutions, Appl. Geochem. 117 (2020) 104601, https://doi.org/10.1016/j.apgeochem.2020.104601.
[24] A. Bukaemskiy, S. Caes, G. Modolo, G. Deissmann, D. Bosbach, Investigation of kinetics and mechanisms of metallic beryllium corrosion for the management of radioactive wastes, MRS Adv. (2024), https://doi.org/10.1557/s43580-024-00835-y.
[25] N. Çevirim-Papaioannou, I. Androniuk, G.D. Miron, M. Altmaier, X. Gaona, Beryllium solubility and hydrolysis in dilute to concentrated CaCl2 solutions: thermodynamic description in cementitious systems, Frontiers Nucl. Eng 2 (2023) 1192463, https://doi.org/10.3389/fnuen.2023.1192463.
[26] K.G. Sheth, J.W. Johnson, W.J. James, The anodic dissolution of polycrystalline Be, Corr. Sci. 9 (1969) 135–144, https://doi.org/10.1016/S0010-938X(69)80024-7.
[27] S. Delpech, C. Cannes, N. Barré, Q.T. Tran, C. Sanchez, H. Lahalle, D. Lambertin, S. Gauffinet, C. Cau-dit-Coumes, Kinetic model of aluminium behavior in cement-based matrices analysed by impedance spectroscopy, J. Electrochem. Soc. 164 (2017) C717–C727, https://doi.org/10.1149/2.0211713jes.